Asymmetric correlation function describing the positional ordering of liquid-phase-epitaxy Si–Ge nanoscale islands

M. Schmidbauer, M. Hanke,* and R. Köhler
Institut für Physik, Humboldt-Universität zu Berlin, Newtonstraße 15, 12489 Berlin, Germany
(Received 16 January 2004; revised manuscript received 21 December 2004; published 25 March 2005)

Liquid-phase-epitaxy grown SiGe nanoscale islands on (001)Si form extended chains which are aligned along the ⟨100⟩ directions. The positional ordering within the island chains was studied by x-ray diffuse scattering. The results can be interpreted by a short-range order model. The corresponding correlation function exhibits an asymmetric peak profile. The asymmetry leads to nonequidistantly spaced satellite peaks that disperse outward slightly with increasing lateral momentum transfer. The observed asymmetric island-island correlation is caused by the successive growth of the islands within a chain, while the new island position is influenced by depletion of the wetting layer around the island.

DOI: 10.1103/PhysRevB.71.115323 PACS number(s): 68.65.−k, 61.10.−i, 81.16.Dn

I. INTRODUCTION

Semiconductor nanoscale islands have been extensively investigated in the last decade.[1] Technological applications of these systems require dense arrays of monodisperse structures of identical shape. Initially, the most widely followed approach to forming nanoscale islands was through electron-beam lithography of suitably small featured patterns. However, besides the fact that the spatial resolution of typically 30 nm is often not small enough, there is still a problem with the large amount of damage introduced during the fabrication process itself. Therefore, self-organized growth mechanisms, such as the Stranski-Krastanow growth mode,[2] have attracted considerable interest. Here, a heteroepitaxial film can release its elastic energy by forming small dislocation-free three-dimensional islands.

Depending on the growth conditions often a well-defined lateral positional ordering of self-assembled nanoscale islands can be observed.[3–6] Type and strength of this ordering can be described by a pair-correlation function. At free-standing islands positional ordering can be investigated by real-space imaging techniques, such as scanning probe microscopy or scanning electron microscopy. Those methods probe the structure locally with high spatial resolution but often with insufficient statistical significance. Therefore, an accurate determination of the pair-correlation function from, e.g., atomic force micrographs, seems to be not feasible. By contrast—owing to typical spot sizes in the range of a few square millimeters—x-ray scattering techniques average statistically over rather large ensembles of islands, and the data are very reliable concerning statistics.

As a result of positional ordering, significant interference of scattered waves from the individual islands may occur and satellite peaks can be observed in the diffuse x-ray scattering. The angular positions of these satellites are related to the mean lateral island distances while the peak widths contain information about a lateral correlation length. Moreover, since the diffuse intensity distribution of the satellite peaks is related to the Fourier transform of the pair-correlation function, a detailed quantitative analysis enables one to distinguish between different types of ordering. Among them are the two limiting cases of short-range order (SRO) and long-range order (LRO), which have been already discussed for positional ordering of quantum dots.[7] In both cases, the satellite peaks are equidistantly spaced in reciprocal space and they vary only in intensity and peak width.

In this paper we discuss the lateral ordering of free-standing $Si_{1-x}Ge_x$ islands, which were grown on (001)Si by means of liquid-phase epitaxy (LPE). A description of the LPE growth procedure can be found elsewhere.[8] Owing to growth conditions close to thermodynamic equlibrium these samples contain highly monodisperse islands of uniform shape and, at sufficiently large island coverage, high positional correlation is observed.[3,9] As an example, atomic force micrographs of $Si_{0.70}Ge_{0.30}$ nanoscale islands are shown in Figs. 1(a) and 1(b). It is very interesting to track the evolution of positional ordering as a function of island coverage. At very low island coverage, there is already a large fraction of islands that are clustered.[3,10] These clusters consist mainly of island dimers, with a small fraction of linear three-island trimers that are oriented along the elastically soft ⟨100⟩ directions. When the island coverage is increased, the dimers and trimers develop into extended rows of islands oriented along ⟨100⟩.[11]

The observed clustering is a clear indication of short-range ordering and suggests that during the growth phase, the nucleation of an island is strongly influenced by already existing islands. However, we will demonstrate that the q dependence of experimental satellite peak positions in the x-ray diffuse scattering indicates that the above-mentioned random-walklike SRO model as used by Stangl *et al.*[7] is not appropriate to correctly describe the lateral ordering of our samples.

II. X-RAY SCATTERING FROM A CORRELATED ENSEMBLE

The investigation of mesoscopic structures by means of x-ray diffuse scattering implies averaging over the illuminating spot size of typically a few square millimeters on the sample. When a single layer of islands with spacings of 100–1000 nm is considered, the number of scattering mesoscopic objects is of order 10^6–10^8, which is a statistically

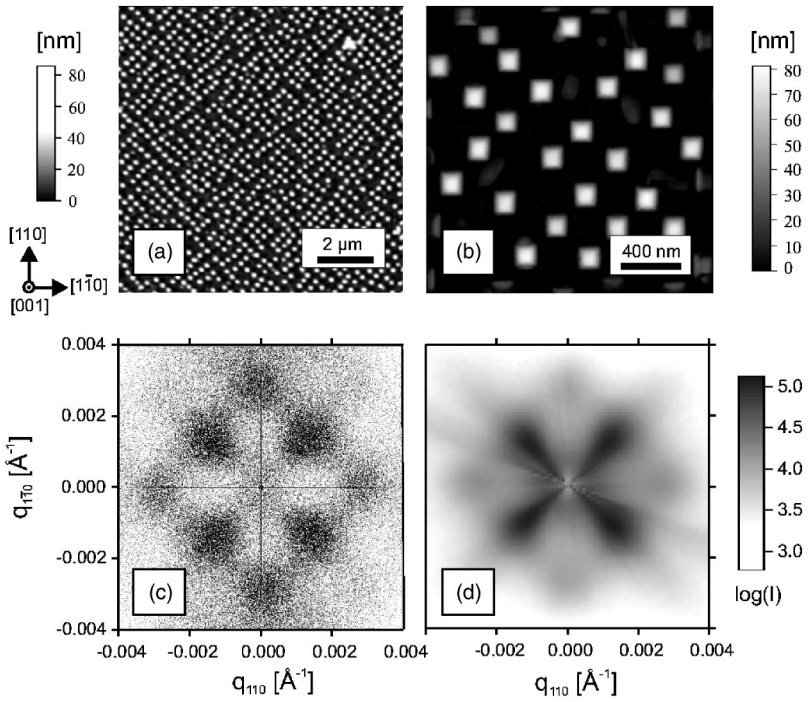

FIG. 1. (a,b) Atomic force micrographs of $Si_{0.70}Ge_{0.30}$ nanoscale islands grown on (001) Si by LPE. The islands are of truncated pyramidal shape with {111} side facets and a (001) top facets. Island base width and height are 130 nm and 65 nm, respectively. The island area coverage is approximately 16%. (c) In-plane AFM power spectrum, (d) GISAXS in-plane intensity distribution.

significant large number. In the case of an ensemble of monodisperse islands of identical shape the diffuse intensity from each individual island is identical. However, the positions of these islands in the ensemble can be correlated, resulting in significant interference of the diffusely scattered waves from the individual islands. Depending on the strength of the positional correlation, this could lead to more or less pronounced and sharp satellite peaks in the diffuse scattering. The distances Δq in reciprocal space between the satellites and the coherent Bragg peak are related to corresponding mean distances $\langle d \rangle$ in real space via

$$\langle d \rangle = \frac{2\pi}{\Delta q}. \tag{1}$$

This equation can be applied to both vertical and horizontal correlation and is very helpful for quickly evaluating experimental data. However, this relationship does not provide information about the details of the correlation function that determines the scattered intensities. Here, we describe how to take account of positional correlation in the framework of kinematical theory. The diffraction from an ensemble of nanoscale islands can be treated such that the scattered amplitudes A_m^{diffuse} from single islands at positions $\mathbf{R}_m$ are (coherently) summed

$$\mathbf{A}_{\text{total}}^{\text{diffuse}}(\mathbf{q}) = \sum_m \mathbf{A}_m^{\text{diffuse}}(\mathbf{q}) e^{i\mathbf{q}\cdot\mathbf{R}_m}, \tag{2}$$

where $\mathbf{q}$ denotes the scattering vector. Note, however, that this expression is valid only if the strain fields of neighboring islands do not remarkably overlap, which is true for the sample discussed here.

For practical reasons, it is impossible to extract useful information about the individual objects when they are different in size, shape, and chemical composition. Extracting information is only possible if all of them are sufficiently similar, i.e., they must have the same shape (including orientation) and at least a narrow size distribution. In the case of identical islands at positions $\mathbf{R}_m$, the amplitudes $\mathbf{A}_m^{\text{diffuse}}(\mathbf{q})$ are also identical and Eq. (2) transforms into

$$\mathbf{A}_{\text{total}}^{\text{diffuse}}(\mathbf{q}) = \mathbf{A}^{\text{diffuse}}(\mathbf{q}) \sum_m e^{i\mathbf{q}\cdot\mathbf{R}_m}. \tag{3}$$

The diffuse intensity from the entire island ensemble can be then written as

$$I(\mathbf{q}) = I(\mathbf{q})_{\text{single}} G(\mathbf{q}), \tag{4}$$

where the interference function is defined as

$$G(\mathbf{q}) = \left| \sum_m e^{i\mathbf{q}\cdot\mathbf{R}_m} \right|^2 = \sum_{m,n} e^{i\mathbf{q}\cdot(\mathbf{R}_m - \mathbf{R}_n)}. \tag{5}$$

In Eq. (5), the summation is performed over the entire ensemble of mesoscopic structures. This requires a knowledge of all island positions $\mathbf{R}_m$, which is practically impossible. Equation (5) should therefore read

$$G(\mathbf{q}) = \left\langle \sum_{m,n} e^{i\mathbf{q}\cdot(\mathbf{R}_m - \mathbf{R}_n)} \right\rangle, \tag{6}$$

where the brackets $\langle\ \rangle$ denote averaging over all possible configurations of the mesoscopic ensemble.

To a certain extent the positions $\mathbf{R}_m$ can be determined by imaging techniques, such as atomic force microscopy (AFM). Here, a sufficiently large area in real space has to be considered. However, the result obtained has to be adapted to the experimental conditions, i.e., the finite coherence of the x-ray beam has to be taken into account. This means that the

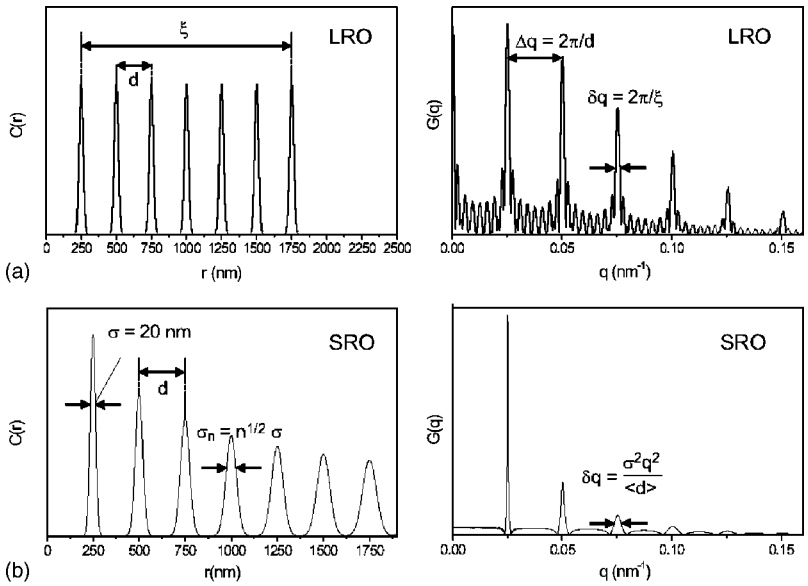

FIG. 2. Autocorrelation function $C(\mathbf{r})$ in real space and the corresponding interference function $G(\mathbf{q})$ in reciprocal space for (a) long-range ordering (LRO), and (b) short-range ordering (SRO) using a random-walklike behavior. For LRO the peak widths and peak spacings of $C(\mathbf{r})$ and $G(\mathbf{q})$ are constant, whereas for SRO the peak widths increase with the peak index. A mean lateral distance of $\langle d\rangle = 250$ nm has been assumed.

coherent sum in (5) has to be taken over those islands that are inside the coherence volume. This sum has then to be averaged over all islands. In other words, the total intensity is calculated by partly coherent and partly incoherent averaging over different subensembles. Recently, this procedure has been successfully applied to SiGe islands.[12]

Equation (4) shows that, as a result of spatial correlation, the diffuse intensity of a single island is modulated by the interference function $G(\mathbf{q})$. Note that $G(\mathbf{q})$ is defined in reciprocal space, whereas the correlation function $C(\mathbf{r})$ is defined in real space. There exists, however, an interesting relationship between $C(\mathbf{r})$ and $G(\mathbf{q})$, which can be obtained by expressing the positions $\mathbf{R}_m$ of the islands in terms of the "island density" through

$$\varrho(\mathbf{r}) = \sum_m \delta(\mathbf{r} - \mathbf{R}_m). \tag{7}$$

Here, the extended size of the mesoscopic structures is neglected and only the mean positions $\mathbf{R}_m$ are considered. By using this relationship for calculating the correlation function

$$C(\mathbf{r}) = \int \varrho(\mathbf{r}')\varrho(\mathbf{r}+\mathbf{r}')dV', \tag{8}$$

we obtain

$$G(\mathbf{q}) = \int C(\mathbf{r})e^{i\mathbf{q}\cdot\mathbf{r}}dV. \tag{9}$$

Thus, the interference function in reciprocal space $G(\mathbf{q})$ is the Fourier transform of the correlation function in real space $C(\mathbf{r})$ and vice versa.

Ordering phenomena are usually discussed in the framework of two limiting models—short-range order (SRO) and long-range order (LRO). For LRO [Fig. 2(a)], the correlation is assumed to be perfect within coherent domains of size ξ [i.e., $C(\mathbf{r})$ exhibits (sharp) peaks of constant width independent of $\mathbf{r}$]. In this case $G(\mathbf{q})$ also shows correlation peaks with constant widths, which are given by Scherrer's formula,[13]

$$\delta q = \frac{2\pi}{\xi}. \tag{10}$$

The domain size ξ can then be interpreted as a correlation length that quantitatively describes the length scale up to which positional correlation is present.

For SRO, the ordering disappears gradually at large distances [Fig. 2(b)]. Therefore the peaks in $C(\mathbf{r})$ become broader and are damped with increasing relative distance r. For the rms peak widths of $C(\mathbf{r})$, Stangl *et al.*[7] have assumed that they behave similar to a random-walk, i.e.,

$$\sigma_n = \sqrt{n}\sigma. \tag{11}$$

Here σ is the rms standard deviation of the mean distance $\langle d\rangle$ between two adjacent islands and is, thus, identical to the peak width of the first correlation peak of $C(\mathbf{r})$. As a consequence of Eq. (11), the peak widths of $G(\mathbf{q})$ also increase with the peak index. They can be expressed as

$$\delta q = \frac{(\sigma q)^2}{\langle d\rangle}, \tag{12}$$

with a correlation length

$$\xi = \frac{\langle d\rangle^3}{2\sigma^2}. \tag{13}$$

Stangl *et al.*[7] have proven the validity of the "random-walk" SRO model for SiGe and PbSe/PbEuTe quantum-dot superlattices. In these systems the degree of ordering is remarkably high, but the SRO behavior is still evident.

The qualitative difference between SRO and LRO is sketched in Fig. 2. In both models the peaks in $G(\mathbf{q})$ are damped for larger q and are equally spaced. Please note that the LRO model employs a finite domain size ξ leading to a

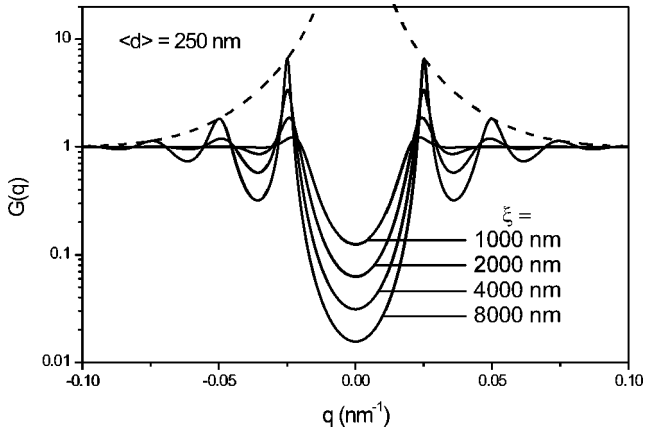

FIG. 3. Calculated interference function $G(q)$ obtained using Eq. (14) for $\langle d\rangle = 250$ nm and various values of the correlation length ξ. The dashed line is the envelope function of the satellite peaks for $\xi = 8000$ nm.

finite, constant peak width of $\delta q = 2\pi/\xi$. By contrast, according to Eq. (12), the peak widths get larger with increasing q for the SRO model.

For the random-walk SRO model as described by Eq. (11), an analytical expression for the interference function $G(\vec{q})$ exists and is given by

$$G(q) = \frac{1 - e^{-\sigma^2 q^2}}{1 + e^{-\sigma^2 q^2} - 2e^{-\sigma^2 q^2/2}\cos(q\langle d\rangle)}. \qquad (14)$$

This expression was developed by Hosemann[14,15] in order to describe scattering in the framework of the so-called paracrystal model. This model attempts to account for both the liquid-like (amorphous) SRO scattering and the sharp diffraction maxima from an LRO structure. The Hosemann function as given in Eq. (14) has been already applied for describing in-plane correlation of free-standing quantum dots.[16,17] Here $\langle d\rangle$ and σ were used as free-fitting parameters. They were treated as anisotropic in real space, since a generalized two-dimensional (in q-space) analytical expression for $G(\mathbf{q})$ does not exist yet.

A very interesting point is the interrelation between $C(\mathbf{r})$ and $G(\mathbf{q})$. What qualitative information can be obtained from the functional behavior of $G(\mathbf{q})$? In the literature (e.g., Ref. 18), the statement can often be found that the presence of many peaks in $G(\mathbf{q})$, i.e., the presence of high-order correlation peaks, can be interpreted as very high correlation. This statement is, however, not generally correct and will be discussed now in more detail. It is certainly true that the degree of ordering is related to the peak width of the first correlation peak, and the corresponding correlation length is given by Eq. (10). This behavior can be inspected in Fig. 3, where calculated values of the interference function $G(q)$ given by Eq. (14) are plotted for different values of ξ. The width of the first correlation peak, indeed, inversely scales with the correlation length ξ. In addition to that behavior, the correlation peaks decay with increasing values of q. The intensity decay can be quantified by an envelope function of the form $(1 + e^{-\sigma^2 q^2/2})/(1 - e^{-\sigma^2 q^2/2})$. The smaller ξ is, the stronger the decay of the correlation peaks. In the SRO model as used in Eq. (11), the appearance of many orders of satellite peaks is thus a sign of high correlation.

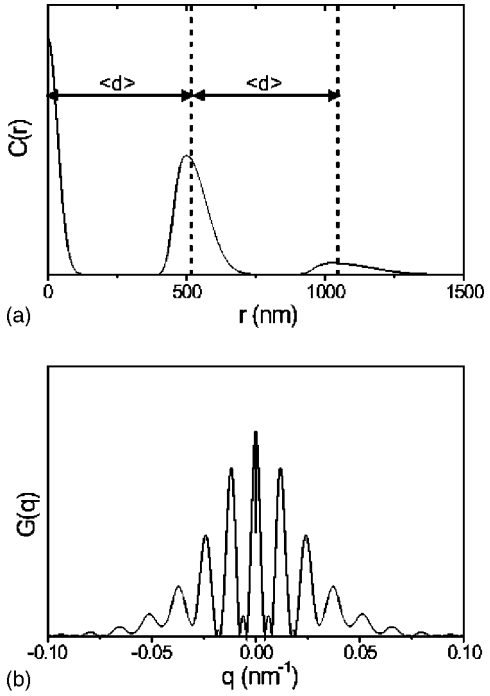

FIG. 4. Calculated autocorrelation (a) and corresponding interference (b) functions $C(\mathbf{r})$ and $G(\mathbf{q}_\parallel)$, for a special SRO model, exhibiting only next-neighbor correlations. A mean distance of $\langle d\rangle = 500$ nm has been assumed. The line shape in $C(\mathbf{r})$ is asymmetric. As a consequence, many high-order correlation peaks are present in $G(\mathbf{q})$ that are not equidistantly spaced but disperse outward slightly with increasing q.

The behavior of SRO discussed above is, however, not generally valid. In Fig. 4, an SRO model where only next-neighbor correlation is present is depicted. When an *asymmetric* peak profile is used for $C(\mathbf{r})$ [Fig. 4(a)] instead of a symmetrical Gaussian distribution, interesting features in the resulting intensity distribution $G(\mathbf{q})$ [Fig. 4(b)] are obtained: (i) Many orders of correlation peaks are present, although rather SRO is present. (ii) The position of the first correlation peak in $G(\mathbf{q})$ is given by $q = (2\pi/\langle d\rangle)$, however, the spacing between neighboring peaks disperse slightly outward. This is a direct consequence of the asymmetric peak profile of $C(\mathbf{r})$.

III. EXPERIMENT

X-ray diffuse scattering intensity distributions were measured in order to probe the interference function $G(q)$ originating from lateral island-island correlation. Two different scattering geometries have been employed, namely, high-resolution x-ray diffraction (HRXRD) and grazing-incidence small-angle x-ray scattering (GISAXS). While GISAXS is solely sensitive to morphological details, such as island shape, size, and spatial correlation, HRXRD additionally probes the lattice strains inside and in the vicinity of the

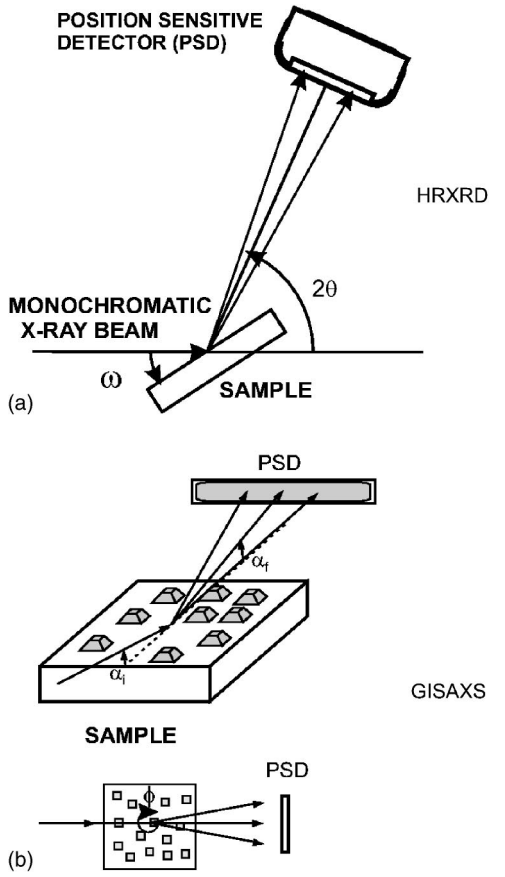

FIG. 5. Experimental scattering geometry for (a) HRXRD and (b) GISAXS. The use of a linear position sensitive detector (PSD) ensures rapid data acquistion.

SiGe islands. Intense synchrotron radiation as provided by the BW2 wiggler station at HASYLAB/DESY has been used in the x-ray scattering experiments. An x-ray wavelength of $\lambda = 1.54$ Å was selected by a Si(111) double-crystal monochromator with a typical bandwidth of $\Delta\lambda/\lambda = 10^{-4}$. A multidetection scattering scheme has been employed in that a linear position-sensitive detector (PSD) was placed at a distance of about 750 mm behind the sample. By using a small spot size of the x-ray beam (typically 100–200 μm) on the sample, each channel of the PSD corresponds to a certain scattering angle.

With HRXRD the PSD is aligned along the 2θ direction [see Fig. 5(a)]. A two-dimensional mapping of the diffusely scattered intensity distribution in reciprocal space can be performed by a single rocking scan (ω scan) of the sample. This procedure ensures fast data acquisition with medium resolution in the scattering plane of typically $\Delta q = 4 \times 10^{-4}$ Å^{-1}. This value—although being definitely worse than the high resolution provided by a crystal analyzer—turned out to be sufficient to clearly resolve satellite peaks in the diffuse scattering. In the direction perpendicular to the scattering plane the resolution is determined by a narrow collimating slit system and amounts to $\Delta q = 3 \times 10^{-3}$ Å^{-1}.

With GISAXS the in-plane diffuse intensity distribution was measured by using a PSD oriented horizontally to the sample surface and by performing azimuthal scans of the sample [Fig. 5(b)]. The measurements have been carried out at glancing angles close to the critical angle of total external reflection. The in-plane resolution typically amounts to $\Delta q = 4 \times 10^{-4}$ Å^{-1}.

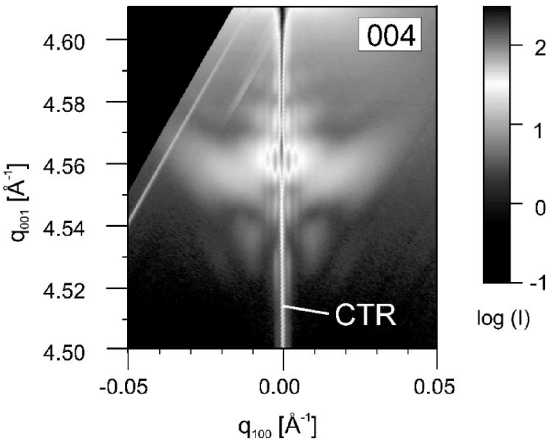

FIG. 6. Measured reciprocal space map (q_{100}-q_{001}-plane) in the proximity of the symmetrical 004 reciprocal lattice point. The Si 004 substrate reflection appears at $q_{001} = 4.628$ Å^{-1} and is not shown here.

The experimental setup and a more detailed description of GISAXS and HRXRD can be found in Refs. 3 and 8, respectively.

IV. RESULTS AND DISCUSSION

For the sample as presented in Figs. 1(a) and 1(b), the two-dimensional nature of the in-plane interference function $G(\mathbf{q})$ can be inspected in Fig. 1(c), where the Fourier transform (power density spectrum) of the AFM height profile [Fig. 1(a)] is displayed. As further discussed in Ref. 3 this spectrum may be directly compared to the GISAXS in-plane intensity distribution, which is depicted in Fig. 1(d). Both AFM and GISAXS clearly show fourfold symmetry with correlation peaks along both the $\langle 100 \rangle$ and $\langle 110 \rangle$ directions. According to Eq. (1) the corresponding mean spacings fulfill the relationship $\langle d_{100} \rangle / \langle d_{110} \rangle = 294/214$ nm $\approx \sqrt{2}$, which demonstrates the development of a square island pattern in real space. However, owing to the low number of islands contributing to the power density spectrum, the AFM investigations suffer from insufficient statistical significance. As a consequence, only the first-order satellite peaks can be detected. This implies that the AFM data cannot be further used for a quantitative evaluation of the interference function $G(\mathbf{q})$. By contrast, X-rays statistically average over a rather large ensemble of islands, making the data very reliable concerning statistics.

In Fig. 6 the measured diffuse intensity (HRXRD) in the vicinity of the symmetrical Si 004 reciprocal lattice point is shown. Here, the scattering plane contains the [100] axis, i.e., the interference function is probed along this direction. The diffuse scattering consists of a rather sharp peak located at about $q_{001} = 4.56$ Å^{-1}, which is surrounded by a characteristic butterfly shaped diffuse feature. The characteristic shape of the intensity distribution is determined by the complex

interplay of strain, local tilts of the atomic planes inside the island, and the island shape function. Comparison to respective x-ray diffuse scattering simulations using elasticity theory could be used to establish the identity of an abrupt vertical Ge composition jump inside the SiGe island.[8,19] In the following we will focus on the lateral positional island correlation and its impact on the diffusely scattered intensity.

In Fig. 6 strong satellite peaks (rods) up to third order are clearly resolved in the immediate proximity of the 00ℓ crystal truncation rod (CTR) of the Si substrate. The q dependence of the satellite peaks is given by the interference function $G(\mathbf{q})$ as defined in Eq. (6). However, as can be inspected in Figs. 1(c) and 1(d), for the AFM in-plane power spectrum and the GISAXS intensity, the interference function $G(\mathbf{q})$ is of a two-dimensional nature, and integration over one direction, as performed by the finite experimental resolution, might affect the experimental intensity distribution. As described in Sec. III the experimental resolution in the q_{010} direction (i.e., perpendicular to the scattering plane) is given by $\Delta q_{010}=3\times10^{-3}$ Å^{-1}. This is still smaller than the distance of the first-order correlation peaks in q_{010} direction, which is given by $\Delta q_{010}=4.3\times10^{-3}$ Å^{-1}. Thus, the intensity distribution as shown in Fig. 1 should not be substantially affected by the experimental integration along q_{010}.

A linear section at $q_{001}=4.560$ Å^{-1} through the experimental intensity distribution shown in Fig. 6 is presented in Fig. 7(a) as open squares. In order to evaluate our data in more detail we have performed a line-shape analysis of our experimental data using Gaussian profiles. Hereby, the smooth strain and shape-induced diffuse scattering has been taken into account by using a broad Gaussian. From this analysis the experimental peak positions of first-, second-, and third-order satellites can be derived with high accuracy as $q_{100}=\pm0.00215$ Å^{-1}, ±0.0045 Å^{-1}, and ±0.0069 Å^{-1}, respectively. Using Eq. (1) the peak position of the first-order satellite corresponds to a mean island-island distance of about $\langle d_{100}\rangle=292$ nm, which fits excellently to the values obtained by GISAXS ($\langle d_{100}\rangle=294$ nm). Comparison to the corresponding AFM micrograph [Fig. 1(a)] shows that this value of $\langle d_{100}\rangle$ corresponds to the island-island distance *within* a chain but is not related to the distance *between* chains.

It is important to mention that, depending on the order, the satellite peaks are not equidistantly spaced but disperse outward slightly with increasing horizontal momentum transfer q_{100}. The observed dispersion cannot be explained within a LRO model or the random-walk SRO model as presented in Fig. 3, where the satellite peak spacings would remain constant. Consequently, the Hosemann function [Eq. (14)] cannot be employed to fit our data.

In order to extract "pure" correlation-related information from the experimental data we have subtracted the shape and strain-induced diffuse scattering, approximated as being Gaussian, from the experimental profile. Also the strong crystal truncation rod at $q_{100}=0$ has been subtracted. The remaining data are then Fourier transformed, and the resulting correlation function $C(r)$ is depicted in Fig. 7(b). Please

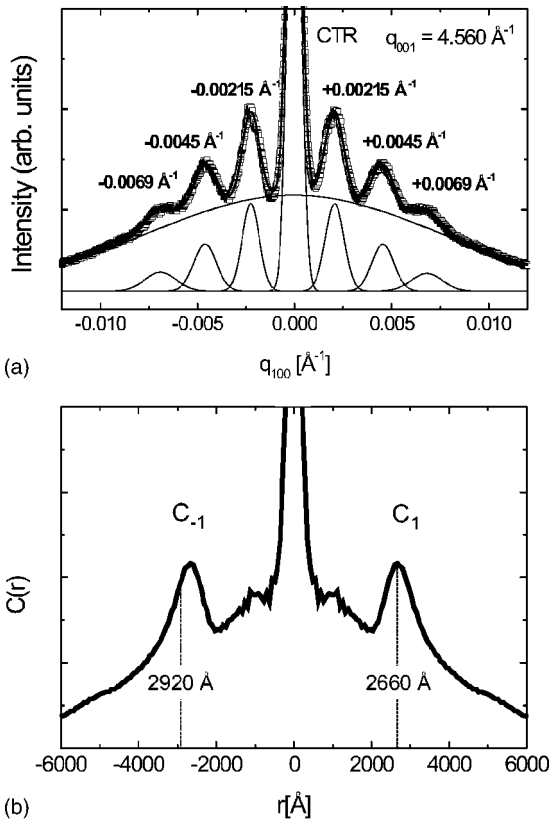

FIG. 7. Measured diffuse intensity of SiGe islands in the vicinity of the 004 reciprocal lattice point: (a) Linear section at $q_{001}=4.560$ Å^{-1} through the experimental intensity distribution shown in Fig. 6. Experimental data are presented as open squares. The solid line represents the best fit to the experimental data using Gaussian line profiles. (b) Corresponding autocorrelation function $C(r)$ in real space. The peak position ($r=266$ nm) and the "center of mass" ($r=292$ nm) of the first correlation peaks $C_{\pm1}$ are marked as dashed lines.

note that, $C(r)$ exhibits only first-order peaks, labeled as $C_{\pm1}$, indicating the presence of SRO.

The peak positions of $C_{\pm1}$ can be evaluated as $r=\langle d_{100}\rangle=\pm266$ nm, respectively, indicating a somewhat smaller mean island distance as evaluated from the first-order satellite peak positions in $G(q)$ and using Eq. (1), which gives $r=\langle d_{100}\rangle=\pm292$ nm. This deviation is caused by the *asymmetric* line profiles of the first-order peaks $C_{\pm1}$. While the peak positions are given by $r=\pm266$ nm, the respective "centers of mass" of $C_{\pm1}$ are located slightly more outward and their positions agree well with $r=\pm292$ nm. Both values for r are marked in Fig. 7(b) as dashed lines.

How can we explain the asymmetric line profile in the autocorrelation function? We would like to emphasize again that the islands are formed *successively*: At early stages of growth dimers and linear trimers of islands are formed, which, at later stages of growth, develop into extended linear island chains oriented along $\langle100\rangle$.[3,10] The linear alignment, thus, takes place by consecutive nucleation of additional islands at the end of an already existing chain. The generation of chains can be explained in terms of minimization of the elastic strain energy during growth[11] and by corresponding

kinetic Monte Carlo simulations.[10] However, these calculations of the elastic strain energy of fully evolved islands do not show any energy minimum along ⟨100⟩ nor any local maximum along the ⟨110⟩ direction, which can lead to an averaged flux of adatoms into the elastically soft direction.[11] However, several papers[20,21] report on the phenomenon that the strain energy around a Stranski Krastanow island can overcompensate the driving forces of growth and even can cause an ablation of deposited material. Indeed, a wetting-layer depletion has been found for LPE SiGe islands, where the depleted area follows exactly the symmetry of strain energy density in the wetting layer.[19] The depletion of the wetting layer impedes adatom nucleation in the immediate vicinity of the island. It is, however, noteworthy that, the depletion for the sample discussed here is so small that it cannot be observed in the AFM image (Fig. 1).

The growth scenario discussed here leads to a strong "island-island repulsion" at distances similar to the island base width, which prevents a growing island to "touch" a fully evolved adjacent island. This can be observed in Figs. 1(a) and 1(b) where the island-island distance within an island chain does not fall below values of about $r \approx 220$ nm, although the island base diagonal width would allow values down to $r = 180$ nm. On the other hand, much larger distances than $\langle d_{100} \rangle = 266$ nm are possible; from the AFM images distances up to about 400 nm are observed, which corresponds to the distance between adjacent island chains. As a consequence of this behavior, an asymmetric distribution of the island-island distances is induced and the profile of the first-order peak in the autocorrelation function becomes asymmetric. The values $r = 220$ nm (minimum island distance) and $r = 400$nm (maximum island distance) observed in the atomic force micrograph are also found in the experimental autocorrelation function [Fig. 7(b)]. At these r values the correlation vanishes. There is thus direct agreement between AFM and corresponding x-ray results.

V. CONCLUSIONS

In conclusion, we have discussed the lateral ordering of SiGe islands grown by LPE on (001)Si. At sufficiently large island area coverage, rows of SiGe islands are formed that extend along the ⟨100⟩ directions. The positional correlation within the island chains has been studied by x-ray diffuse scattering and atomic force microscopy. Although high orders of satellite peaks can be observed, the results can be explained by a short-range order model. The corresponding correlation function shows an asymmetric peak profile. This, in addition, leads to nonequidistantly spaced satellite peaks, which disperse outward slightly with increasing q.

The observed asymmetric island-island correlation is caused by the successive growth of the islands within a chain. This means that the next island is always formed at the end of an already existing chain. The position of the new island is presumably determined by depletion of the wetting layer around the islands, which exactly follows the shape of the strain energy density. Therefore, the distribution of the islands around the most probable value $\langle d_{100} \rangle = 266$ nm is asymmetric. The distances within the chains cannot be smaller than about $r \approx 220$ nm, however, much larger values up to $r = 400$ nm are possible.

ACKNOWLEDGMENTS

We thank our co-workers H. Raidt and P. Schäfer for valuable discussions and assistance with the experiment. We are also thankful to H. Wawra (Institut für Kristallzüchtung, Berlin) for providing us with the SiGe sample. Finally, we gratefully acknowledge technical support by the HASYLAB staff. This work was partly supported by "Deutsche Forschungsgemeinschaft" within the framework of Sfb 296.

*Present address: Fachbereich Physik, Martin-Luther-Universität Halle-Wittenberg, Hoher Weg 8, D-06120 Halle/Saale, Germany.

[1] D. Bimberg, M. Grundmann, and N. N. Ledentsov, *Quantum Dot Heterostructures* (Wiley, Chichester, NY, 1999).
[2] I. Stranski and L. Krastanow, Sitzungsber. Akad. Wiss. Wien, Math.-Naturwiss. Kl., Abt. 2B **146**, 797 (1937).
[3] M. Schmidbauer, T. Wiebach, H. Raidt, M. Hanke, R. Köhler, and H. Wawra, Phys. Rev. B **58**, 10 523 (1998).
[4] F. Hatami, U. Müller, H. Kissel, K. Braune, R.-P. Blum, S. Rogaschewski, H. Niehus, H. Kirmse, W. Neumann, M. Schmidbauer *et al.*, J. Cryst. Growth **216**, 26 (2000).
[5] G. Springholz, V. Holý, M. Pinczolits, and G. Bauer, Science **282**, 734 (1998).
[6] Y. I. Mazur, W. Q. Ma, X. Wang, Z. M. Wang, G. J. Salamo, M. Xiao, T. D. Mishima, and M. B. Johnson, Appl. Phys. Lett. **83**, 987 (2003).
[7] J. Stangl, T. Roch, V. Holý, M. Pinczolits, G. Springholz, G. Bauer, I. Kegel, T. H. Metzger, J. Zhu, K. Brunner *et al.*, J. Vac. Sci. Technol. B **18**, 2187 (2000).
[8] T. Wiebach, M. Schmidbauer, M. Hanke, H. Raidt, R. Köhler, and H. Wawra, Phys. Rev. B **61**, 5571 (2000).
[9] M. Schmidbauer, T. Wiebach, H. Raidt, M. Hanke, R. Köhler, and H. Wawra, J. Phys. D **32**, 230 (1999).
[10] M. Meixner, E. Schöll, M. Schmidbauer, H. Raidt, and R. Köhler, Phys. Rev. B **64**, 245307 (2001).
[11] M. Hanke, H. Raidt, R. Köhler, and H. Wawra, Appl. Phys. Lett. **83**, 4927 (2003).
[12] M. Hanke, M. Schmidbauer, and R. Köhler, J. Appl. Phys. **96**, 1959 (2004).
[13] A. Guinier, *X-Ray Diffraction* (Freeman, San Francisco, 1968).
[14] R. Hosemann, Z. Phys. **128**, 1 (1950).
[15] R. Hosemann and S. N. Bagchi, *Direct Analysis of Diffraction by Matter* (North-Holland, Amsterdam, 1963).
[16] I. Kegel, T. H. Metzger, J. Peisl, P. Schittenhelm, and G. Abstreiter, Appl. Phys. Lett. **74**, 2978 (1999).
[17] V. Chamard, T. H. Metzger, E. Bellet-Amalric, B. Daudin, C.

Adelmann, H. Mariette, and G. Mula, Appl. Phys. Lett. **79**, 1971 (2001).
[18] K. Zhang, C. Heyn, W. Hansen, T. Schmidt, and J. Falta, Appl. Phys. Lett. **76**, 2229 (2000).
[19] M. Hanke, M. Schmidbauer, D. Grigoriev, H. Raidt, P. Schäfer, R. Köhler, A.-K. Gerlitzke, and H. Wawra, Phys. Rev. B **69**, 075317 (2004).
[20] X. Z. Liao, J. Zou, D. J. H. Cockayne, J. Qin, Z. M. Jiang, X. Wang, and R. Leon, Phys. Rev. B **60**, 15 605 (1999).
[21] U. Denker, O. G. Schmidt, N. Y. Jin-Phillip, and K. Eberl, Appl. Phys. Lett. **78**, 3723 (2001).